Journal of Southeast University (English Edition) Vol. 32, No. 2, pp. 187 - 194 June 2016 ISSN 1003—7985

Online frequency and power regulation scheme of magnetic coupled resonant wireless power transfer

Tan Linlin Yan Changxin Huang Xueliang Wang Wei Jing Wuwei

(School of Electrical Engineering, Southeast University, Nanjing 210096, China)

Abstract: In order to address the issues that the magnetic coupled resonant wireless power transfer (MCR-WPT) system is sensitive to the resonant frequency and that transmission power is difficult to control with the non-resistive load in the MCR-WPT, a single-side regulation scheme for frequency and transmission power online is proposed, which is based on the inherent constraint relationships the among system parameters in the primary side. Thus, the communication between the primary side and the secondary side is avoided. First, the transfer models of resistance-capacitance load and resistance-inductance load are established, respectively. Next, the relationship between the input voltage phasor and the input current phasor is used to recognize the load property and value. Then, the coaxial rotation of the stepper motor and the rotating vacuum variable capacitor is conducted to unify resonant frequency both in the primary side and the secondary side. Finally, the regulations of both frequency and amplitude of input voltage are made to guarantee transmission power under a new resonant frequency point the same as the one when the only pure resistance part of load is accessed under the former resonant frequency point. Both simulation and experimental results indicate that the proposed regulation scheme can track resonant frequency and maintain transmission power constant.

Key words: magnetic coupled resonant; frequency regulation; power regulation; non-resistive load

doi: 10.3969/j.issn.1003-7985.2016.02.010

Magnetic coupled resonant wireless power transfer (MCR-WPT), introduced by the MIT team in 2007[1], has attracted much attention from academic section both at home and abroad. Honored for one of the key future technologies by American *Technology Review* in 2008, this technology has been primarily utilized for smart domestic appliances, electric vehicles, mobile terminals and implanted medical devices[2-4].

Due to the fact that MCR-WPT has a longer transfer distance than inductive power transfer (IPT), it has a wider application and brighter prospects in contrast to IPT[5-8]. Usually, high quality factor Q is employed in coils to enlarge the transfer distance and improve transfer efficiency. However, in this case, on the one hand, system performance such as frequency characteristic and energy-selection become more incisive, which consequently undermines the stability and robustness of the system[9]. On the other hand, load access is restrained in terms of value and property because the load value is related to impedance match[10-11] and the load property determines whether the system can operate on the designed resonant frequency or not.

A resistor accessing the system can guarantee the system operation on the designed resonant frequency. However, the system characteristics will be varied once the load property changes. For example, resistance-inductance or resistance-inductance load access mistunes the system and thus affects the transmission power of the system. Much research has been done on a frequency control[12-18], such as a frequency control scheme via phase lock loop (PLL). Unfortunately, those works cannot realize the frequency regulation over a wide range and the load recognition on the primary side at the same time.

In order to reduce the complexity of the system, this paper proposes an online regulation scheme for both frequency and power on the primary side. The scheme is fulfilled in three stages. First, the load property and its value are recognized through relationship of the input voltage phasor and the input current phasor. Secondly, the primary-side compensative capacitor is regulated to retune the system with the co-axial rotation of the stepper motor. Thirdly, the frequency and amplitude of the input voltage are controlled to maintain transmission power constant.

1 Modeling and Analysis

1.1 Retuning model for resistance-inductance load or resistance-capacitance load

Either the resistance-inductance load access or resistance-capacitance load access will change the designed resonant frequency. Fig. 1 depicts the equivalent circuit of the system, where U_s is the alternative source on the primary side; R_1 and R_2 are the internal resistances of the

Received 2015-10-12.

Biographies: Tan Linlin (1986—), male, doctor, lecturer; Huang Xueliang (corresponding author), male, doctor, professor, xlhuang@seu.edu.cn.

Foundation items: The National Natural Science Youth Foundation of China (No. 51507032), the Natural Science Foundation of Jiangsu Province (No. BK20150617), the Fundamental Research Funds for the Central Universities.

Citation: Tan Linlin, Yan Changxin, Huang Xueliang, et al. Online frequency and power regulation scheme of magnetic coupled resonant wireless power transfer[J]. Journal of Southeast University (English Edition), 2016, 32(2): 187 - 194. doi: 10.3969/j.issn.1003-7985.2016.02.010.

transmitting and receiving coil, respectively; C_1, C_2 and L_1, L_2 represent the compensative capacitance and equivalent inductance on the primary side and secondary side, respectively; M stands for the mutual inductance between the transmitting coil and receiving coil; and Z_L represents the load. It is well known that with resistive load access (namely Z_L has a real part solely), the system operates on the designed resonant frequency ω_0 based on the MCR-WPT theory. Whereas, either the resistance-inductance load access or resistance-capacitance load access alters ω_0.

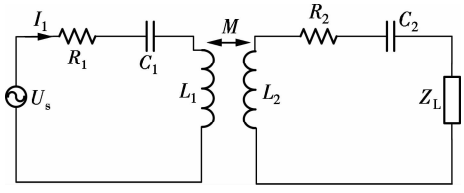

Fig. 1 MCR-WPT equivalent circuit

In the following part, the analysis for resonant frequency is carried out under both the resistance-inductance load and resistance-capacitance load access cases.

In the resistance-inductance load access case, assuming that $Z_L = R_L + j\omega L$, the resonant angular frequency in the secondary side can be derived as

$$\omega_1 = \frac{1}{\sqrt{(L_2 + L)C_2}} \tag{1}$$

The system must be retuned to guarantee the consistent resonant frequency both on the primary and secondary sides. Here in this paper, the parallel variable capacitor C_{x1} in transmitting coil is introduced, as shown in Fig. 2, to enlarge the equivalent capacitor on the primary side.

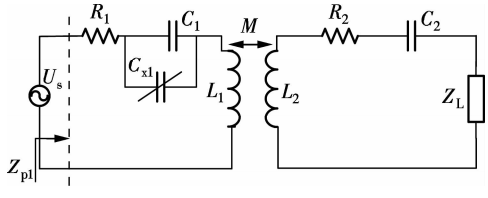

Fig. 2 Diagram with parallel retuning capacitor

Hence, with the angular frequency ω_0, the total impedance Z_{p1} on the primary side can be expressed as

$$Z_{p1}(\omega_0) = R_1 + j\omega_0 L_1 - j\frac{1}{\omega_0(C_1 + C_{x1})} + \frac{(\omega_0 M)^2}{R_2 + j\omega_0 L_2 - j\dfrac{1}{\omega_0 C_2} + R_L + j\omega_0 L} \tag{2}$$

Substituting angular frequency ω_1 into Eq. (1),

$$Z_{p1}(\omega_1) = R_1 + j\omega_1 L_1 - j\frac{1}{\omega_1(C_1 + C_{x1})} + \frac{(\omega_1 M)^2}{R_2 + R_L} \tag{3}$$

In order to calculate the variable capacitor C_{x1}, the imaginary part of Z_{p1} is set to be zero, namely,

$$\omega_1 L_1 - \frac{1}{\omega_1(C_1 + C_{x1})} = 0 \tag{4}$$

Therefore, C_{x1} can be calculated as

$$C_{x1} = \frac{1}{\omega_1^2 L_1} - C_1 \tag{5}$$

Similarly, in the resistance-capacitance load access case, assuming that $Z_L = R_L - j\dfrac{1}{\omega C}$, the new tuning angular frequency can be described as

$$\omega_2 = \sqrt{\frac{C + C_2}{L_2 C_2 C}} \tag{6}$$

The variable capacitor in transmitting coil retunes the frequency, as illustrated in Fig. 3, to decrease the equivalent capacitor on the primary side.

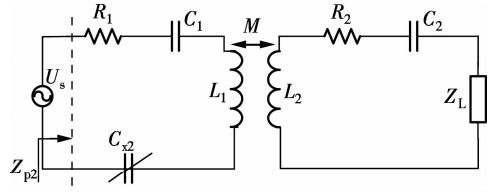

Fig. 3 Diagram with series retuning capacitor

Similarly, with the angular frequency ω_0, Z_{p2} is expressed as

$$Z_{p2}(\omega_0) = R_1 + j\omega_0 L_1 - j\frac{1}{\omega_0 C_1} - j\frac{1}{\omega_0 C_{x2}} + \frac{(\omega_0 M)^2}{R_2 + j\omega_0 L_2 - j\dfrac{1}{\omega_0 C_2} + R_L - j\dfrac{1}{\omega_0 C}} \tag{7}$$

Substituting angular frequency ω_2 into Eq. (6), we obtain

$$Z_{p_2}(\omega_2) = R_1 + j\omega_2 L_1 - j\frac{1}{\omega_2 C_1} - j\frac{1}{\omega_2 C_{x2}} + \frac{(\omega_2 M)^2}{R_2 + R_L} \tag{8}$$

Then, similarly, to calculate C_{x2}, the imaginary part of Z_{p2} is set to be zero as

$$\omega_2 L_1 - \frac{1}{\omega_2 C_1} - \frac{1}{\omega_2 C_{x2}} = 0 \tag{9}$$

and C_{x2} is

$$C_{x2} = \frac{C_1}{\omega_2^2 L_1 C_1 - 1} \tag{10}$$

By the theoretical analysis above, the consistent resonant frequency on two sides can be realized by variable capacitor C_x, which is in parallel or in series with the former compensative capacitor on the primary side under resistance-inductance load access or resistance-inductance load access. Moreover, the values of C_x are given in Eqs. (5) and (10), respectively.

1.2 Power regulation model under resistance-inductance and resistance-capacitance load access

As aforementioned, retuning the system aims to main-

tain resonant situation so as to improve the transfer efficiency and power factor. Furthermore, in order to effectively promise the stability of power transfer, some power regulation schemes must be applied on the primary side following the frequency regulation.

The initial condition of the system is presented as follows: the input voltage $u_s = \sqrt{2}\,U_0 \sin(\omega t)$; load $Z_L = R_L$ and the resonant angular frequency is ω_0; the transmission power can be computed as

$$P_L(\omega_0,\ U_0) = \frac{U_0^2 \omega_0^2 M^2 R_L}{(R_1 R_2 + R_1 R_L + \omega_0^2 M^2)^2} \tag{11}$$

The principle of power control is to maintain transmission power P_L constant. When $Z_L = R'_L + jX_L$ and the system is retuned, the transmission power can be deduced as

$$P_L(\omega,\ U) = \frac{U^2 \omega^2 M^2 R'_L}{(R_1 R_2 + R_1 R'_L + \omega^2 M^2)^2} \tag{12}$$

Maintain P_L a constant, i.e., $P_L(\omega,\ U) = P_L(\omega_0,\ U_0)$, then the target amplitude of the input voltage can be described as

$$U = \sqrt{\frac{R_L}{R'_L}}\,\frac{\omega_0}{\omega}\,\frac{R_1 R_2 + R_1 R'_L + \omega^2 M^2}{R_1 R_2 + R_1 R_L + \omega_0^2 M^2} U_0 \tag{13}$$

Therefore, with the load change, the transmission power can be maintained constant by the input voltage regulation.

1.3 Online acquisition of parameters for frequency and power regulation

Elaborated in both 1.1 and 1.2, the corresponding parameters should be acquired to implement frequency and power regulation. The phase difference between the input voltage and the input current is zero under the resonant condition. Hence, the input impedance with no load change and the angular frequency being ω_0 can be represented as

$$Z_{in} = R_1 + \frac{(\omega_0 M)^2}{R_L + R_2} \tag{14}$$

where R_1 and R_2 are determined by the coils and they scarcely change while R_L is in the list of to-be-acquired parameters. Due to the fact that Z_{in} can be calculated by the input voltage U_0 and the input current I_1, then the load R_L can be computed as

$$R_L = \frac{(\omega_0 M)^2}{Z_{in} - R_1} - R_2 = \frac{(\omega_0 M)^2}{U_0 / I_1 - R_1} - R_2 \tag{15}$$

Leading or lagging phase difference between the input voltage and the input current will occur with the change in load property and here δ stands for the phase difference. Before retuning the system, the angular frequency of the system is ω_0 and the real part and imaginary part of Z_{in} are, respectively, shown as

$$\mathrm{Re}Z_{in} = Z_{in}\cos\delta = \frac{U_0}{I_1}\cos\delta = R_1 + \frac{(\omega_0 M)^2 (R_2 + R'_L)}{(R_2 + R'_L)^2 + X_L^2} \tag{16}$$

$$\mathrm{Im}Z_{in} = Z_{in}\sin\delta = \frac{U_0}{I_1}\sin\delta = \frac{-(\omega_0 M)^2 X_L}{(R_2 + R'_L)^2 + X_L^2} \tag{17}$$

In Eqs. (16) and (17), the variables R'_L and X_L, and R'_L can be computed as

$$R'_L = \frac{(U_0\cos\delta - I_1 R_1) I_1 \omega_0^2 M^2}{(U_0\sin\delta)^2 + (U_0\cos\delta - I_1 R_1)^2} - R_2 \tag{18}$$

In addition, due to the fact that X_L represents either the inductive load or the capacitive load, then its corresponding inductance L or corresponding capacitance C can be derived as

$$L = \frac{\omega_0 M^2 U_0 I_1 \sin\delta}{(U_0\sin\delta)^2 + (U_0\cos\delta - I_1 R_1)^2} \tag{19}$$

$$C = \frac{(U_0\sin\delta)^2 + (U_0\cos\delta - I_1 R_1)^2}{\omega_0^3 M^2 U_0 I_1 \sin\delta} \tag{20}$$

Thus, the target value of C_x and voltage U can be calculated.

The phase difference δ can be measured by the zero-crossing time difference between the input voltage and the input current and Δt stands for zero-crossing time difference. Therefore, under the angular frequency ω_0, the phase difference δ is equal to $\omega_0 \Delta t$.

2 Control Scheme and Flow for Retuning and Power

Based on the aforementioned mathematical analysis and the control method, the changes both in load value and property will be calculated by examining the input voltage phasor and the input current phasor including their amplitudes and phase difference. As a result, on the one hand, the system can be retuned by regulating the compensative capacitor in the primary side. On the other hand, the transmission power can be kept constant by regulating the input voltage.

There are two methods to vary the compensative capacitor on the primary side as reported in the released literature. One is the capacitor matrix, which manifests different capacitances through different capacitance assemblies[19]. Feasible as it is, its design and control scheme are complicated. The other is the phase-controlled capacitor or inductor. The equivalent inductor and capacitor will change via the switching technique. Simple as it is, this method will produce large harmonics.

In this paper, change in the primary-side compensative capacitor is realized by the co-axial rotation of the stepper motor and the rotating vacuum variable capacitor, as shown in Fig. 4, where A and B are the wiring terminals of the vacuum capacitor. The stepper motor in Fig. 4 contains 2 phases with 12 steps per round. Moreover, according to the manufacturer's instructions, the vacuum

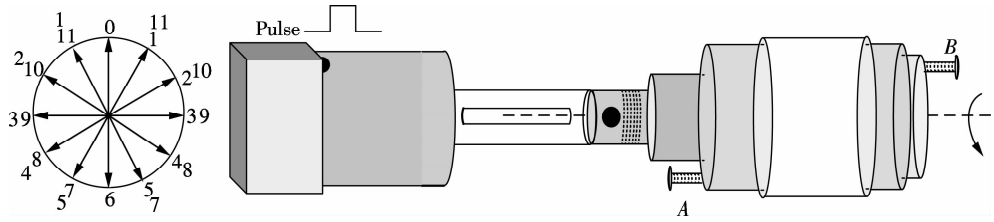

Fig. 4 Co-axis rotation of stepper motor and vacuum capacitor

capacitor C is described as

$$C = \frac{\varepsilon S}{4\pi kd} \tag{21}$$

where S is the effective counterpart square of two electrode plates of the capacitor; d is the distance between these two plates; k is the static electricity constant; and ε is the relative dielectric constant. In particular, C is proportional to S. The curve of C vs. S is shown in Fig. 5 from the manufacturer's instruction. Consequently, the changes in S driven by the stepper motor can be depicted in Fig. 6. Here, S in Eq. (21) can be described by

$$S = 2\pi rh \tag{22}$$

where r is the internal radius of vacuum capacitor; h stands for the effective height of the counterpart plates, thus

$$\Delta S = 2\pi r\Delta h \tag{23}$$

Moreover, the change of Δh can be made by the co-axial rotation of the stepper motor and the vacuum capacitor and thus, Δh can be derived as

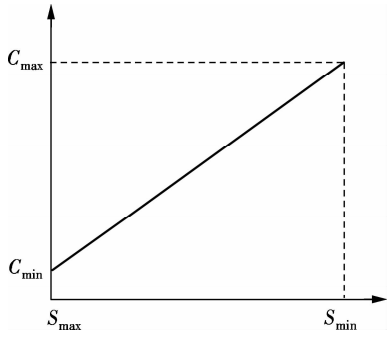

Fig. 5 Curve of capacitor C and square S

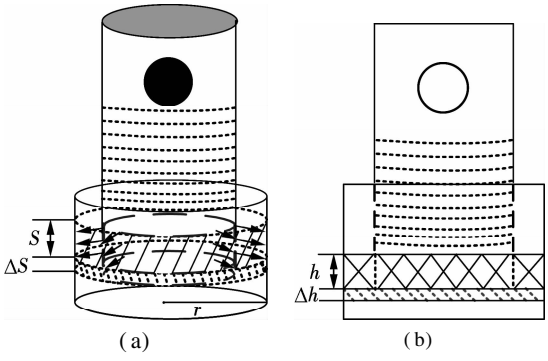

Fig. 6 Schematic picture of vacuum capacitor. (a) Schematic diagram; (b) Main view diagram

$$\Delta h = \frac{N}{12}\text{pit} \tag{24}$$

where N is the number of the rotation step; pit represents the pitch of the screw in the axis of the vacuum capacitor. Δh finally causes change in C as

$$\Delta C = \frac{\varepsilon rN\text{pit}}{24kd} \tag{25}$$

Either increasing or decreasing step number will cause the equivalent square S to change, which finally results in the change of C value. As a result, shown in Fig. 7, with the rotation of the stepper motor, the capacitor C will vary.

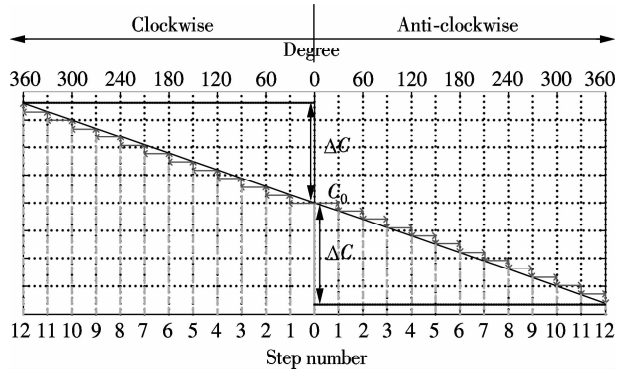

Fig. 7 Equivalent capacitor changes with stepper motor rotation

The property and value of the load Z_L are examined and calculated by the amplitude and phase difference of the input voltage U_s and the input current I_1. δ stands for the phase difference between the input voltage and the input current. In detail, $\delta > 0$ indicates that the current phasor leads the voltage phasor, and vice versa; $\delta < 0$ suggests that the current phasor lags behind the voltage phasor. For example, on the one hand, $\delta > 0$ means that resistance-inductance load accesses the system and the driving signal makes the stepper motor rotate clockwise so as to increase the equivalent C to retune the system. Following that, the input voltage will be regulated to maintain the transmission power constant. On the other hand, $\delta < 0$ indicates that the resistance-capacitance load accesses the system and the pulse is generated to drive the stepper motor to rotate in anti-clockwise direction to decrease the equivalent C to retune the system frequency. Then, similarly, the input voltage will be changed to ensure that the transmission power remains constant. The control block diagram and control flow diagram are illustrated in Figs. 8(a) and (b), respectively.

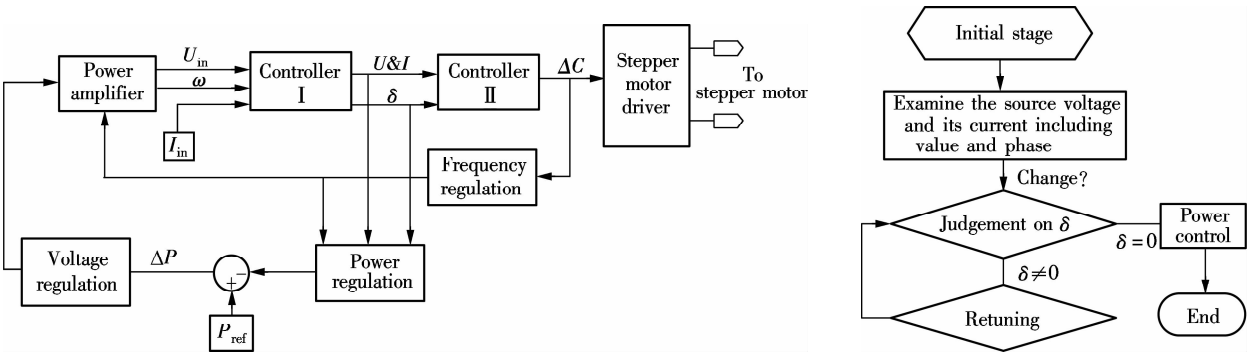

(a) (b)

Fig. 8 Control block diagram and control flow diagram for tuning and active power stability. (a) Control block diagram; (b) Control flow chart

3 Simulation and Prototype

In order to validate the feasibility of the proposed regulation scheme for retuning and stabilizing transmission power, simulation models established in Matlab Simulink and prototype experiments are conducted (see Fig. 9). The parameters of the simulation are tabulated in Tab. 1.

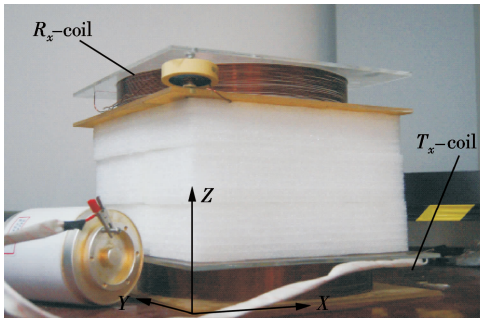

Fig. 9 Prototype of MCR-WPT system

Tab. 1 System simulation parameters

Parameters	Value
L_1, L_2/μH	350
C_1, C_2/ pF	300
R_1, R_2/Ω	0.11
M_{12}/μH	20
ω_0/kHz	491
R_L/Ω	100
R_s/Ω	50

Fig. 10 shows the initial condition of the MCR-WPT system, (a) and (b) are the simulated and measured waveforms of input voltage and input current, respectively. As shown in Fig. 10, the RMS of input voltage is 29 V, the RMS of input current is 0.29 A and δ is zero. The resonant frequency is 491 kHz and the transmission power is 8.7 W. However, with an unknown load access in the system, the waveforms are shown in Fig. 11.

In Figs. 11(a) and (b), $\delta<0$ means that the resistance-capacitance load accesses in the system and the input frequency is also 491 kHz. The RMS of input voltage is about 28 V (a small decrease compared to the initial condition caused by internal resistance). But the RMS of input current rises to 1.12 A and δ is about 85°. More importantly, the transmission power is 2.4 W, having decreased by 72%. Therefore, according to Eqs. (16) and (17), $R=100\ \Omega$, $X_c=-648\ \Omega$, and namely C in load is 500 pF. Based on the above analysis, the new resonant frequency is 621 kHz, and the RMS of the input voltage has to be regulated to 35 V to maintain a consistent transmission power. Fig. 12 shows that the waveforms in the resonant frequency is 621 kHz and that the transmission power is 8.8 W.

Furthermore, in order to validate whether the proposed control scheme is suitable for all kinds of load access, given the initial condition of the system as shown in Fig. 10, waveforms in Fig. 13 indicates that another kind of load accesses the system.

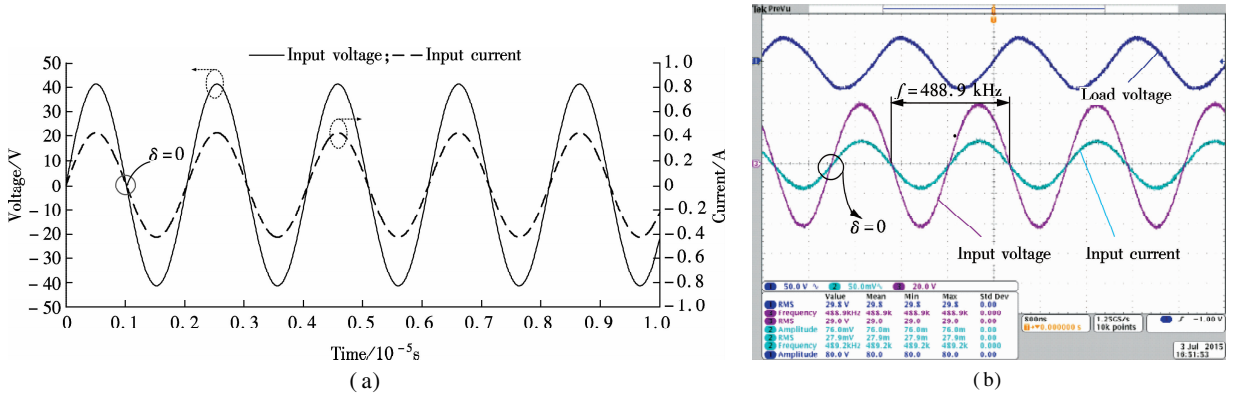

(a) (b)

Fig. 10 Waveforms under the initial condition of the MCR-WPT system. (a) Simulated; (b) Experimental

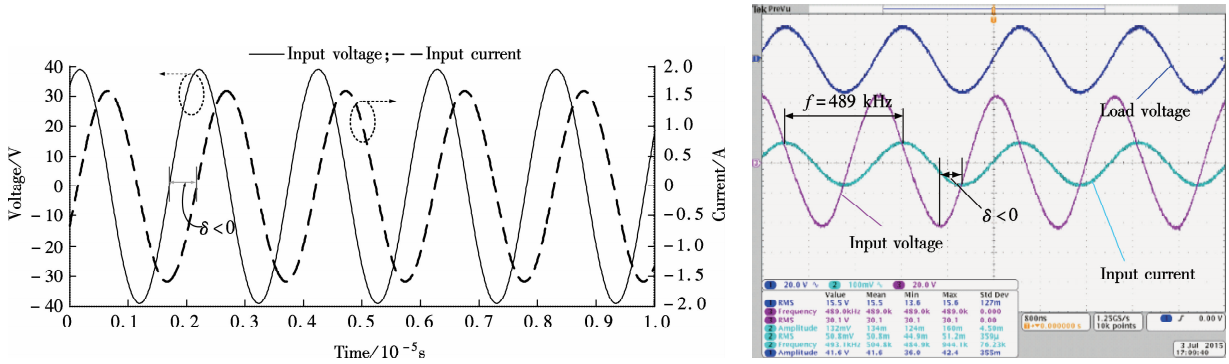

Fig. 11 Waveforms of unknown load in the system with $\delta<0$. (a) Simulated; (b) Experimental

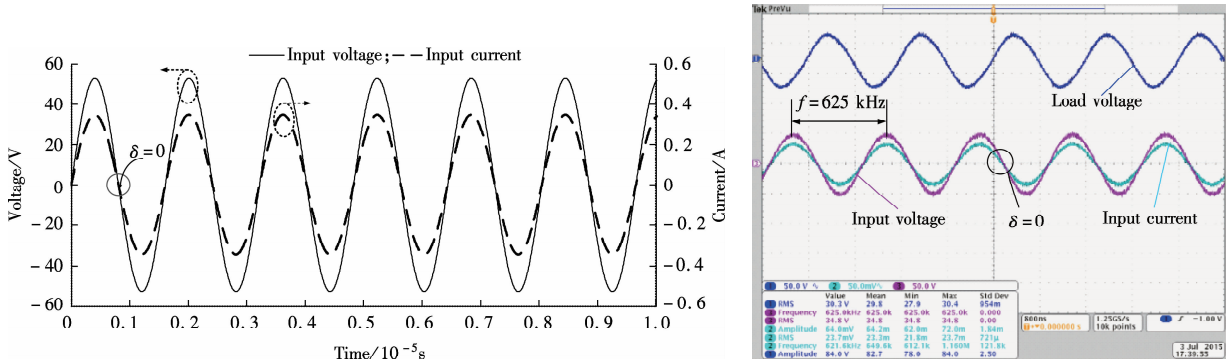

Fig. 12 Waveforms under the new resonant condition with resistance-capacitance load access. (a) Simulated; (b) Experimental

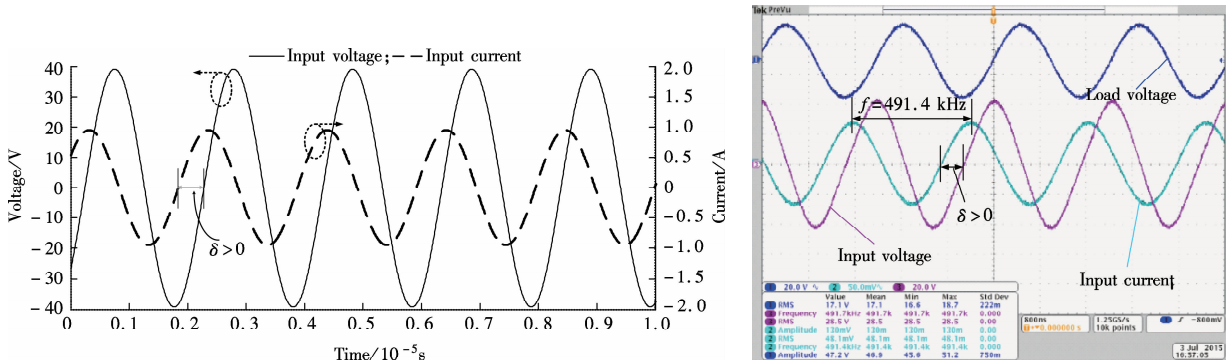

Fig. 13 Waveforms of unknown load in the system with $\delta>0$. (a) Simulated; (b) Experimental

Similarly, in Figs. 13(a) and (b), $\delta>0$ means that the resistance-inductance load accesses in the system, the input frequency is also 491 kHz and that the RMS of the input voltage is about 28 V (a small decrease compared to the initial condition caused by internal resistance). However, the RMS of the input current increases to 0.67 A and δ is about 65°. More importantly, the transmission power is 2.9 W, having decreased by 67%.

Therefore, according to Eqs. (16) and (17), $R=100\ \Omega$, $X_L=309\ \Omega$, namely L is 100 μH. Based on the above analysis, the new resonant frequency is 433 kHz, and the RMS of the input voltage has to be regulated to 21 V to maintain consistent transmission power. Fig. 14 shows the waveforms in the resonant frequency of 433 kHz and the transmission power is 8.8 W.

In summary, both the simulation and experiment validate the feasibility of the proposed method. The retuning frequency and power control can be applied to a wide range of load access with high accuracy.

Finally, it should be noticed that various factors including the voltage and frequency band of the power amplifier, the mutual inductance of the two coils can exert effect on the regulation range of both the resonant frequency and voltage, which actually affect the resistance-inductance load access margin or resistance-capacitance load access margin. In this paper, the effect of the power amplifier is discussed and the mutual inductance is seen as a constant.

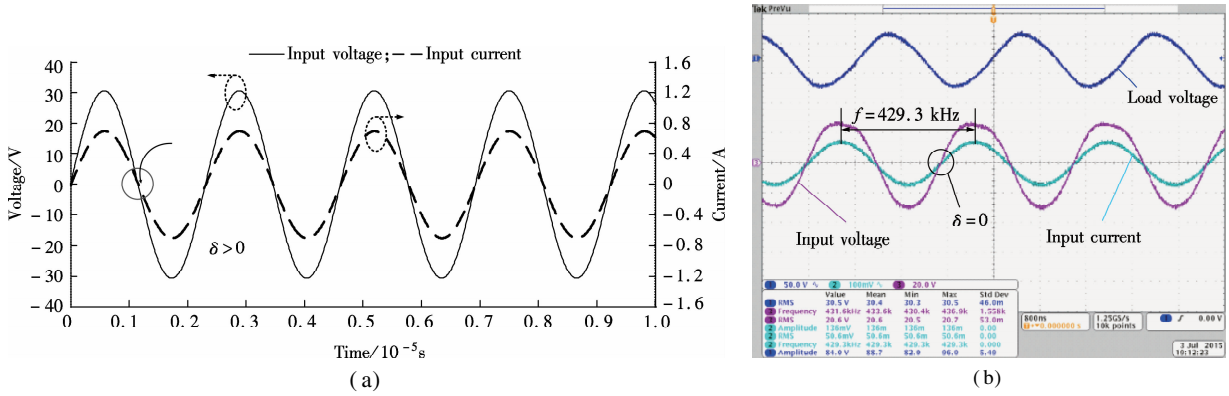

Fig. 14 Waveforms under the new tuning condition with resistance-inductance load access. (a) Simulated; (b) Experimental

Assume that $f_{\max}$, $f_{\min}$ are the upper limit and lower limit of the frequency band of the power amplifier, respectively; $U_{\max}$ and $U_{\min}$ represent the upper limit and lower limit of the voltage control of the power amplifier, respectively. In addition, the real part of Z_L is a constant, namely, R_L. Hence,

$$U_{f_{\max}} = \frac{f_0}{f_{\max}} \frac{R_1R_2 + R_1R_L + 4\pi^2 f_{\max}^2 M^2}{R_1R_2 + R_1R_L + 4\pi^2 f_0^2 M^2} U_0$$

$$U_{f_{\min}} = \frac{f_0}{f_{\min}} \frac{R_1R_2 + R_1R_L + 4\pi^2 f_{\min}^2 M^2}{R_1R_2 + R_1R_L + 4\pi^2 f_0^2 M^2} U_0$$

Usually, the frequency range of the alternative source is from several hundred kHz to several MHz. In our experiment, $U_0 = 40$ V, $f_{\min} = 100$ kHz, $f_{\max} = 1$ MHz, $U_{\min} = 20$ V and $U_{\max} = 100$ V. Thus, $U_{f_{\max}} = 2.03U_0 = 81.2$ V, $U_{f_{\min}} = 0.217U_0 = 8.68$ V. Consequently, the effective voltage control range is from 20 to 81.2 V. Accordingly, the effective frequency regulation range is from 245 kHz to 1 MHz. Therefore, the maximum inductance in the load that can be accessed is 1 044 μH and the minimum accessed capacitance in the load is 100 pF.

4 Conclusion

In this paper, the model for online retuning and power control is established via the mathematic analysis of the effects that either resistance-inductance load access or resistance-capacitance load access exerts on resonant frequency and transmission power. The proposed method is to examine the amplitude of the input voltage and input current and their phase difference so as to recognize the load property and compute the value of load. Moreover, system retuning depends on the primary-side variable compensative capacitor which is in co-axial rotation with a stepper motor and power control relies on the regulation of the input voltage's amplitude and frequency. The advantage of the method is that there is no need to collect the parameters on the secondary side, and retuning through co-axial rotation of the vacuum capacitor and stepper motor can achieve high accuracy. Simulation and experiments validate the feasibility of the proposed control scheme.

References

[1] Kurs A, Karalis A, Moffatt R, et al. Wireless power transfer via strongly coupled magnetic resonances [J]. *Science*, 2007, **317**(5834): 83 – 86. DOI: 10.1126/science.1143254.

[2] Zhao Z, Zhang Y, Chen K. New progress of magnetically-coupled resonant wireless power transfer technology [J]. *Proceedings of the Chinese Society of Electrical Engineering*, 2013, **33**(3): 1 – 13.

[3] Yang Q. Research progress in contactless power transmission technology [J]. *Transactions of China Electrotechnical Society*, 2010, **25**(7): 6 – 13.

[4] Hui S Y R, Zhong W, Lee C K. A critical review of recent progress in mid-range wireless power transfer [J]. *IEEE Transactions on Power Electronics*, 2014, **29**(9): 4500 – 4511. DOI: 10.1109/tpel.2013.2249670.

[5] Bani S M, Kawamura A, Yuzurihara I, et al. A wireless power transfer system optimized for high efficiency and high power applications [C]//2014 *International Power Electronics Conference*. Hiroshima, Japan, 2014: 2794 – 2801. DOI: 10.1109/ipec.2014.6870077.

[6] Cheon S, Kim Y H, Kang S Y, et al. Circuit-model-based analysis of a wireless energy-transfer system via coupled magnetic resonances [J]. *IEEE Transactions on Industrial Electronics*, 2011, **16**(7): 2906 – 2914. DOI: 10.1109/tie.2010.2072893.

[7] Garnica J, Casanova J, Lin J. High efficiency midrange wireless power transfer system[J]. *Environment & Development Economics*, 2011, **16**(16): 73 – 76.

[8] Dionigi M, Franceschetti G, Mongiardo M. Resonant wireless power transfer: investigation of radiating resonances[C]//2013 *IEEE Wireless Power Transfer*. Perugia, Italy, 2013: 17 – 20.

[9] Zhang Y, Zhao Z. Frequency splitting analysis of two-coil resonant wireless power transfer[J]. *IEEE Antennas & Wireless Propagation Letters*, 2014, **13**(4): 400 – 402.

[10] Lim Y, Tang H, Lim S, et al. An adaptive impedance-matching network based on a novel capacitor matrix for wireless power transfer [J]. *IEEE Transactions on Power Electronics*, 2014, **29**(8): 4403 – 4413. DOI: 10.1109/tpel.2013.2292596.

[11] Bou E, Sedwick R, Alarcon E. Maximizing efficiency through impedance matching from a circuit-centric model of non-radiative resonant wireless power transfer [C]//

2013 *IEEE International Symposium on Circuits and Systems*. Beijing, China, 2013: 29 – 32. DOI: 10. 1109/iscas. 2013. 6571774.

[12] Tan L L, Huang X L, Huang H, et al. Transfer efficiency optimal control of magnetic resonance coupled system of wireless power transfer based on frequency control[J]. *Science China Technological Sciences*, 2011, **54**(6): 1428 – 1434. DOI: 10. 1007/s11431-011 – 4380-6.

[13] Tan L L, Huang X L, Zhou Y L, et al. Optimal control of wireless energy transfer system via decreasing frequency [J]. *Journal of Southeast University* (*English Edition*), 2013, **29**(3): 259 – 263.

[14] Huang X L. Study on series-parallel model of wireless power transfer via magnetic resonance coupling [J]. *Transactions of China Electrotechnical Society*, 2013, **28**(3): 171 – 176.

[15] Zhang W, Wong S C, Tse C K, et al. Design for efficiency optimization and voltage controllability of series-series compensated inductive power transfer systems [J]. *IEEE Transactions on Power Electronics*, 2014, **29**(1): 191 – 200. DOI: 10. 1109/tpel. 2013. 2249112.

[16] Sakemi G, Yoshimura T, Fukuda N. A study of optimization for efficiency and power control in an electromagnetic WPT system[C]//2013 *IEEE International Meeting for Future of Electron Devices*. Kansai, Japan, 2013: 108 – 109.

[17] Gundogdu A E, Afacan E. The effect of frequency, multi resonator and relay resonator conditions on wireless power transmission[C]//*Wireless Telecommunications Symposium* (*WTS*). London, UK, 2012: 1 – 5.

[18] Zhang W, Wong S C, Tse C K, et al. Design for efficiency optimization and voltage controllability of series-series compensated inductive power transfer systems [J]. *IEEE Transactions on Power Electronics*, 2014, **29**(1): 191 – 200. DOI: 10. 1109/tpel. 2013. 2249112.

[19] Sun Y, Wang Z H, Dai X, et al. Study of frequency stability of contactless power transmission system[J]. *Transactions of China Electrotechnical Society*, 2005, **20**(11): 56 – 59.

磁耦合谐振式无线电能传输系统功频在线调节策略

谭林林　颜长鑫　黄学良　王　维　景无为

（东南大学电气工程学院，南京 210096）

摘要：为了解决磁耦合谐振式无线电能传输系统频率特性尖锐及非阻性负载接入时传输功率难以控制的问题，基于系统初级侧参数固有的约束关系，提出了一种单侧功-频在线控制策略，从而避免两侧之间建立通讯. 分别建立系统在阻容性和阻感性负载接入时的传输模型，利用初级侧输入电压相量和输入电流相量的关系对负载性质和大小进行辨识；利用步进电机和初级侧真空可调电容的共轴旋转调整容值以使得初级侧谐振频率和次级侧谐振频率一致；调节输入电压频率和幅值以保持系统在新的谐振频率点下传输功率与在原谐振频率点下仅接入该负载阻性部分时的传输功率一致. 仿真和实验结果表明，所提出的控制策略能够准确地实现谐振频率的跟踪和传输功率的恒定.

关键词：磁耦合谐振；频率调节；功率调节；非阻性负载

中图分类号：TM133